Rayón, E.; Arrieta, MP.; Pasies -Oviedo, T.; López-Martínez, J.; Jorda Moret, JL. (2018). Enhancing the mechanical features of clay surfaces by the absorption of nano-SiO2 particles in aqueous media. Case of study on Bronze Age clay objects. Cement and Concrete Composites. 93:107-117. https://doi.org/10.1016/j.cemconcomp.2018.07.005

Enhancing the mechanical features of clay surfaces by the absorption of nano-SiO_2 particles in aqueous media. Case of study on Bronze Age clay objects

E. Rayón[a*], M.P. Arrieta[b], T. Pasíes[c], J. López[a], J.L. Jordá [d]

[a)] Instituto de Tecnología de Materiales. Universitat Politècnica de Valencia. Camí de Vera s/n. E46022. Valencia. Spain

[b)] Instituto de Ciencia y Tecnología de Polímeros. Consejo Superior de Investigaciones Científicas (ICTP-CSIC). Calle Juan de la Cierva 3, 28006, Madrid. Spain

[c)] Museo de Prehistoria de Valencia. Corona 36, E-46003 Valencia. Spain

[d)] Instituto de Tecnología Química, Universitat Politècnica de València, Consejo Superior de Investigaciones Científicas, Avenida de los Naranjos s/n, Valencia, Spain

***CORRESPONDIG AUTHORS**:

Emilio Rayón Encinas

Instituto de Tecnología de Materiales (UPV)

Cami de Vera s/n. E-46022

e-mail. emraen@upvnet.upv.es

Phone: (+34) 660806113

Abstract

Nanoparticles are known to be able to enhance the performance of low dense materials, achieving the small intergranular spaces to further interact with the matrix. In this work, we propose a study on the use of nano-SiO_2 particles dispersed in an aqueous medium as a treatment to improve the mechanical surface's resistance of an ancient clay material. Several low-strength clay fragments dated from the Bronze Age were surface treated with a commercial aqueous suspension of nano-SiO_2 particles. FESEM images suggest that nanoparticles, of 20 nm diameter, filled the inter-granular spaces of the

clay. The improvement of the mechanical properties of surfaces was corroborated by the nanoindentation technique, showing that the nanohardness and elastic modulus increased from 15 to 150 MPa and from 1 to 8 GPa, respectively.

Keywords: surface treatment, SiO_2 nanoparticles, nanoindentation, heating reaction diffractometer, microstructure, mechanical properties.

1. Introduction

The laboratories of heritage museums are constantly looking for new products to improve the conservation-restoration of historic heritage objects [1-7] such as ancient ceramics and clays [8-12] as well as new approaches to the measurement of the level of consolidation (mechanical performance), of those treated objects. In this context, from a conservation point of view, results of fundamental importance to increase the mechanical performance of ancient pieces; not only because they are in general fragile materials, but also because they should be maintained for long periods of time. It is widely known that an effective strategy to improve the resistance and the mechanical properties of materials, is to achieve certain grade of nanostructuration [13-15]. In the restoration field of ancient ceramics that is their effective consolidation. Nanocomposite materials have demonstrated good mechanical performance due to the high specific surface area of nanoparticles that increases the physical interactions inside the material at the nanometer scale [16]. Nowadays, it is increasing the interest of conservation-restoration community to explore possible treatment procedures by using nanoparticles on a non-nanostructured ancient material in order to confer new functionalities with improved properties [17-19] .

The consolidation procedure consists on a treatment in which a consolidating (strengthener) substances is applied [3, 5, 20]. The treatment can be applied to the entire

volume of the piece or only on its surface or in certain localized areas. When the treatment affect to the surfaces the visual aspect must always be kept as identical as possible to untreated pieces. Other characteristics that the consolidating substance must present are water permeability, absence of harmful secondary products and be non-toxic for secure manipulation, which is not always possible due to the volatile character of these organic products [21].

The most common products used to consolidate ancient ceramics or clay materials are synthetic resins and the well-known ethyl silicate [22, 23]. Nowadays, there is a trend to use safer and harmless products based on aqueous mediums. Protective coatings containing SiO_2 are widely used to protect materials mainly from corrosion, chemical reactions and mechanical damage [24]. In this context SiO_2 particles with dimensions at the nano-level scale are better on the improvement of the mechanical performance even at low concentration loadings as a consequence of their small particle size [25]. In this context, there are some novel commercial aqueous suspensions based on dispersed SiO_2 nanoparticles that has been proposed as interesting nanoreinforcement for coatings applications [26] and also to treat stone, ceramic and clay surfaces [17].

This work aims to explore the possibility to confer to heritage pieces of better superficial mechanical performances and to subsequently study the effectiveness of the treatment. This case of study was performed on ancient clay fragments of the Bronze Age found in the Lloma of Betxí in Paterna, Valencia (Spain) based on a surface treatment with dispersed SiO_2 nanoparticles. The consolidating substance used was characterized by Transmission Electron Microscopy, while the composition of the clay piece was studied by Energy Dispersive X-ray (EDS). The microstructure of the untreated and treated clay pieces was studied by optical and Field Emission Electron

Microscopy (FESEM). The efficiency of the treatment on the mechanical performance of the ancient clay pieces was analyzed by several analyses such as nanoindentation and scratch tests, which were performed to determine the surface hardness, elastic modulus and scratch resistance properties. Furthermore, the possible colour changes caused by this treatment were also evaluated in the CIELab space.

2. Experimental details

2.1. Archaeological material

Samples analyzed in this study were unearthed in a Bronze Age settlement located in the 'Lloma of Betxí' in the city of Paterna, province of Valencia (Spain) [27]. In this excavation 28 pieces, almost all in small fragments, were discovered [28]. Fig. 1 shows a picture of some of found pieces. These pieces correspond to loom weights with a characteristic rectangular geometry and four through holes. The estimated dating of the artifacts agrees with the existence of an intensive textile industry in this location. However, the weight measured for each piece was in the range between 1.800 and 2.000 g. This moderate weight leads to think that these pieces were used in stranding of fibers techniques or in winding machines [28]. The stability of pieces seems adequate considering the brittle character of the clay whereas their surfaces present a very low resistance against low friction forces. The analyzed and treated samples in this study were disjointed fragments.

Fig. 1. Image of the Bronze Age loom weights

2.2. Strengthening treatment

A commercial Nano Estel suspension (C.T.S., Italy) was used to consolidate the surfaces of the clay pieces. Nano Estel is a colloidal aqueous suspension of SiO_2 nanoparticles. The most important characteristics reported by the product manufacturer are water permeability when dried, compatibility with the original material, not producing secondary products, short drying times, nontoxic, safe and harmless. The suspension was stabilized by the supplier with NaOH (<0.5%) giving to the suspension a strong alkaline character (pH: 9.8-10.4). Table 1 summarizes the chemical and physical properties of the suspension used in this study.

In this work two treatments with this suspension were conducted, one using a diluted solution in distilled water (15wt% of nano-SiO_2), and another using the suspension as-delivered (30wt% of nano-SiO_2). Samples were immersed in the nanoSiO_2 colloidal suspension at room temperature for 15 minutes to reach a good absorption. Then, the samples were introduced inside a vacuum chamber for 2 hours.

Subsequently, the samples were drained and the excess liquid was absorbed using a desiccant paper. Previous to the microstructural and nanomechanical analysis, samples were kept at 24ºC and 55% relative humidity inside a climatic chamber for 1 month. Four untreated fragments and another four fragments of each treatment (4+8 samples) were analyzed.

Table 1. Summary of the physical and chemical properties of the commercial nano-SiO_2 suspension.

Nano Estel specifications	**Physical and chemical properties**
Solid material	SiO_2
Appearance	Colourless liquid
Solid content	30 wt%
Viscosity	7 mPa s at 20 ºC
Density	1.2 g / cm^3 at 20 ºC
Particle dimension	< 20 nm
Specific surface	260 m^2 / g
pH	10

2.3. Microstructure and elementary chemical analysis

The microstructure of the cross-section of samples was analyzed by an optical reflection microscope, Leica M125 from Leica Microsystems, under a coaxial illumination system powered by a KL1500 LCD illuminator. Previous to observation, a convenient polishing metallographic procedure was performed with abrasive papers.

A JEOL Transmission Electron Microscope (TEM), Model JEM-1010, was used to characterize the morphology of the suspension solid content. A drop of the

suspension was poured on a copper grid holder. After several minutes in air, the solvent had evaporated spontaneously and the sample could then be analyzed.

The microstructure of the surface and the cross section of the nanocomposites formed after the consolidating treatment, were observed by a Zeiss Oxford Field Emission Electron Microscope (FESEM), model Ultra 55. Samples were coated with Pt-Au. Elementary analysis was performed in the same equipment by using an energy dispersive X-ray (EDS) detector under 20 kV acceleration.

2.4. Structural analysis

The crystalline structure of the material at room temperature was determined by powder X-ray diffraction with a PANalytical X'Pert PRO diffractometer using Cu Kα radiation. For non-ambient measurements, the sample was heated in an Anton-Parr XRK-900 reaction chamber attached to the diffractometer.

2.5. Surface colour properties

An HP Scanjet 8300 professional image scanner was used to evaluate the possible change of the colour properties by measuring colour coordinates in the CIELab colour space. The instrument was calibrated with a white and black standard tiles. Results were expressed as colour coordinates L (lightness), a* (red-green) and b* (yellow-blue). Total colour differences (ΔE) induced by the Nano Estel treatments were calculated with respect to untreated clay by using Equation 1:

$$\Delta E = \sqrt{\Delta L^2 + \Delta a^{*2} + \Delta b^{*2}} \qquad \text{Equation 1}$$

153

154 Statistical analysis of differences in colour parameters were studied by one-way analysis
155 of variance (ANOVA) using OriginPro 8 software. In order to identify which groups
156 were significantly different from other groups, mean value comparisons were done
157 employing a Tukey's test with a 95% confidence level.

158

159 *2.6. Nanomechanical analysis*

160 Hardness (H) and elastic modulus (E) were acquired with a G-200 nanoindenter
161 (Agilent Technology, USA). The indenter consisted of a Berkovich geometry tip
162 previously calibrated on silica as a reference material. An array of 25 indentations with
163 a 150 μm distance between them was performed at a 2000 nm depth. The Continuous
164 Stiffness Measurement (CSM) was set at 2 nm harmonic oscillation amplitude and a 45
165 Hz oscillation frequency. This mode provides the in-depth stiffness profile and, hence,
166 allows the subsequent calculation of H and E [29].

167 Nanoscratch tests were performed using the same nanoindenter. Three scratches
168 were performed on each sample. Fig. 2 shows a schematization of the scratch test
169 conditions in this test. In order to scratch and record the features of the resulting groove,
170 (i) the indenter was loaded to a very low value (100μN) to assure contact with the
171 surface of sample. The tip scans the original surface topography over the entire scratch
172 path. This pre-profile is used to level all the subsequent scratch cycles. Then, the
173 indenter returns to the origin of the acquired pre-profile path in order to reach the initial
174 scratch position. After that, the indenter is ramp-loaded from 0 to 2.5 mN at a 10μm/s
175 scratch velocity, scratching a path of 300 μm length. When the scratch segment is
176 completed, the stages are moved back to the origin of the scratch path and the indenter
177 load is decreased to 100 μN. A subsequent post-profile path of the region just past the

scratch path is registered (this data is represented as a residual groove topography plot). Finally, a cross-profile scan of the path is recorded by moving the stages to the 150 µm cross profile position and then the cross profile is initiated applying a constant 0.1 mN scan load.

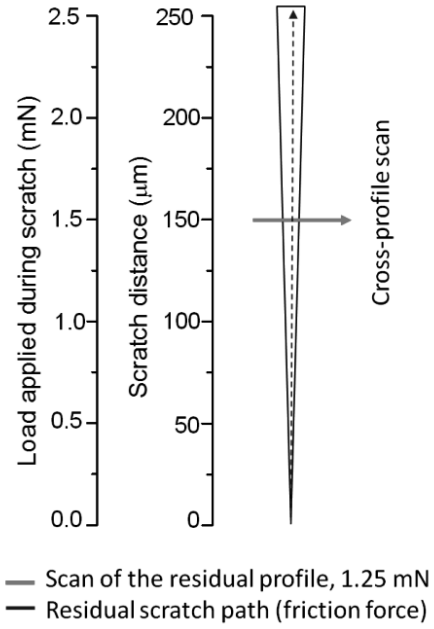

Fig. 2. Scheme of the scratch sequence and experimental conditions used

3. Results and Discussion

3.1. Material characterization

The microstructure, elementary and compositional analysis of samples was conducted previous the treatment study. The Fig. 3 shows a representative image of the cross-section view of a conveniently polished sample. The material presents a high porosity with dimensions ranging from 500 to 2000µm, approximately. Inside the pores, it was common to find mineralized vegetable fibers.

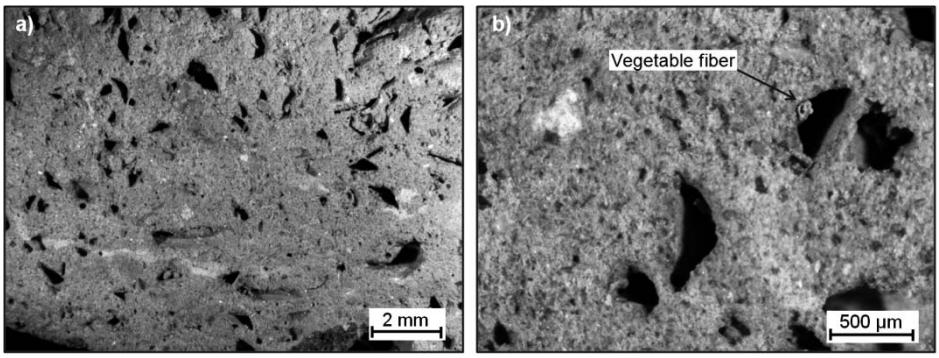

Fig. 3. Optical microscopy image of the clay cross-section fragments at 50x and 75x magnifications.

A preliminary elemental analysis by EDS of the material in form of debris extracted from untreated pieces revealed the common chemical composition of a clay based material, revealing traces of Al, Mg, Fe and Ca (Table 2).

Table 2. Elemental analysis results of the clay material obtained by EDS-FESEM

Element	Weight%	Atomic%
Mg	1.46	1.32
Al	10.58	8.58
Si	24.71	19.25
K	4.23	2.37
Ca	10.48	5.72
Fe	3.34	1.31
O	44.80	61.27

According to the X-ray diffraction peaks observed for the original sample (Figure 4), the material is constituted by a mixture of Low Quartz (SiO_2), Calcite ($CaCO_3$) and monoclinic Muscovite 2M1 ($H_2KAl_3Si_3O_{12}$). These results are in good agreement with

205 the chemical analysis obtained from EDS-FESEM. The presence of Fe and Mg can be
206 attributed to a partial substitution of those elements in the structure of muscovite. The
207 presence of calcite in the material and the absence of peaks corresponding to lime (CaO)
208 suggest that the sample was originally heated at temperatures below 600ºC.

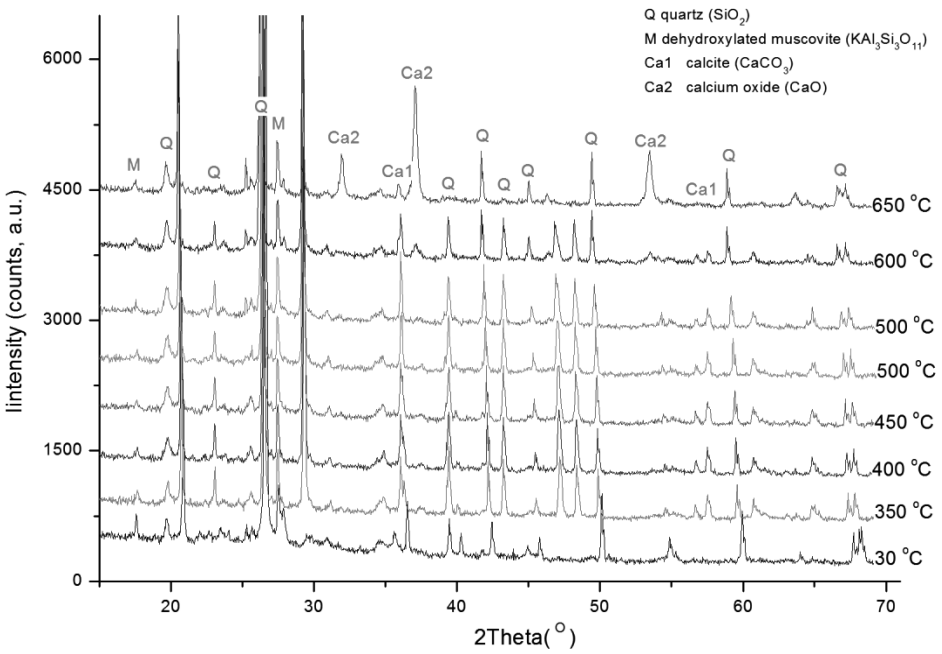

209

210 **Fig. 4.** DRX spectrum of the powder extracted from the Bronze Age clay pieces.

211

212 In order to clarify a possible ancient cooking, the material was heated *in situ* in a dry air
213 atmosphere. The X-ray difractograms were acquired in the range from 350 to 600ºC. As
214 it can be observed, the peaks corresponding to quartz remain unaltered during the whole
215 process, while the layers of muscovite expand along their stacking direction, being that
216 process reversible after cooling again at room temperature. However, at 650ºC it is
217 observable an irreversible decomposition of calcite ($CaCO_3$) to form lime (CaO). This
218 reaction corroborates that these pieces were probably not cooked or heated above
219 600ºC, it agreement with the observed presence of mineralized vegetal fibers.

220

221 *3.2. Microstructural characterization of the nanoparticle consolidating suspension*

The solid content of the suspension was analyzed by means of TEM. The images showed in Fig. 5, captured at several magnifications, display spherical nanoparticles. The measured diameters were in the range of 10 to 20 nm corroborating the nanometric character of the solid content.

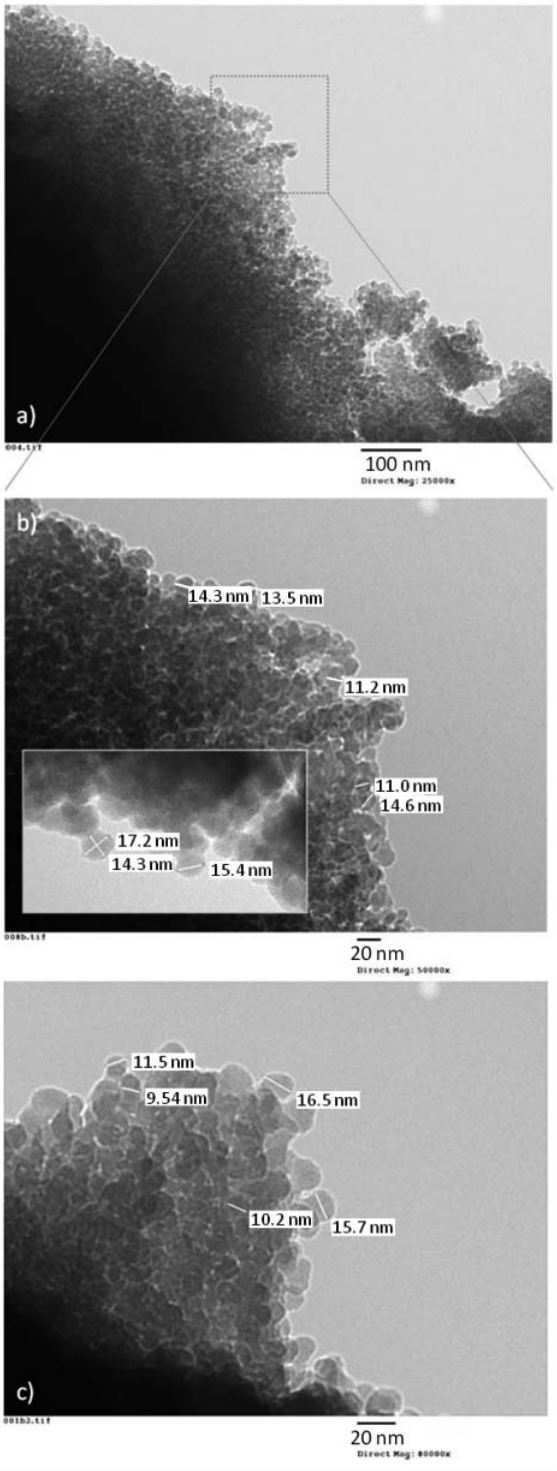

Fig. 5. TEM images of the nano-SiO_2 nanoparticles under several magnifications (suspension was dried on carbon coated copper grid).

3.3. Characterization of samples.

This characterization study was focused on a comparative analysis of untreated specimens and treated samples. The study was focused in the surface regions of samples.

3.3.1. Microstructural characterization

The optical study of the surface of the untreated and treated samples exhibits several differences, as can be seen in Fig. 6 Meanwhile the untreated sample (Fig. 6-a and c) evidences a material without a consolidated surface (grains of clay are flyaway), the treated samples show a consolidated surface without observable free particles (Fig. 6b and d). However, a thin cracked transparent film was found on the sample treated with 30% of solid content (Fig. 6d). This residue is attributed to an excess of silica due to the bad absorption that is probably caused as a consequence of the high viscosity of the non-diluted suspension. This observation suggests that it is necessary to dilute the colloidal suspension.

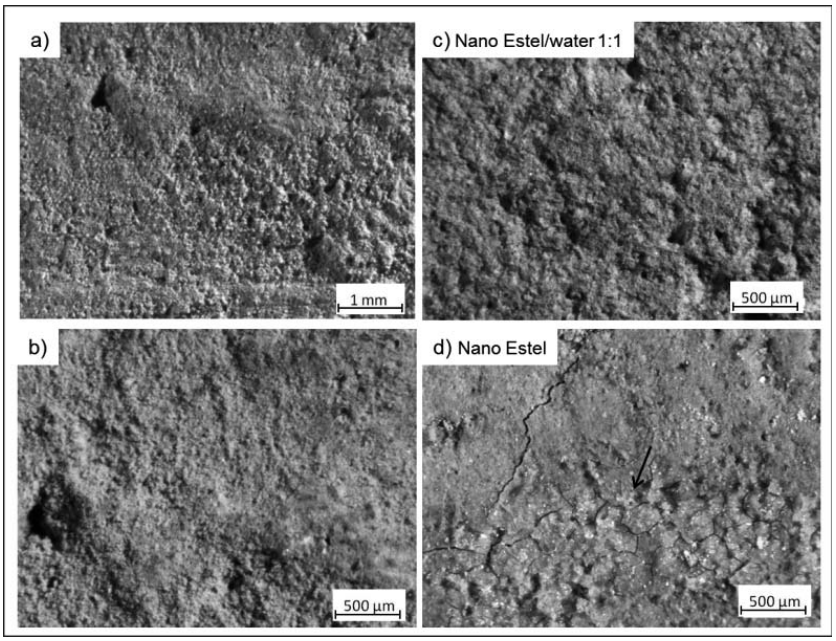

Fig. 6. Optical microscopy images of the clay surfaces a, b) without treatment, c) after treatment with aqueous 15%wt nano-SiO_2 and d) after treatment with aqueous 30%wt nano-SiO_2.

In depth analysis of the microstructure of untreated piece was performed by FESEM. The Fig. 7-A shows captured images of the untreated clay piece at two magnifications. Well defined polygonal and laminar thin grains characteristic of this compositional clay are observed. These grains seem poorly bonded by the basal planes and the resultant material is then easy delaminated, presenting the observed fragile character. Furthermore, the lack of integrity is favored by the low dense material observed.

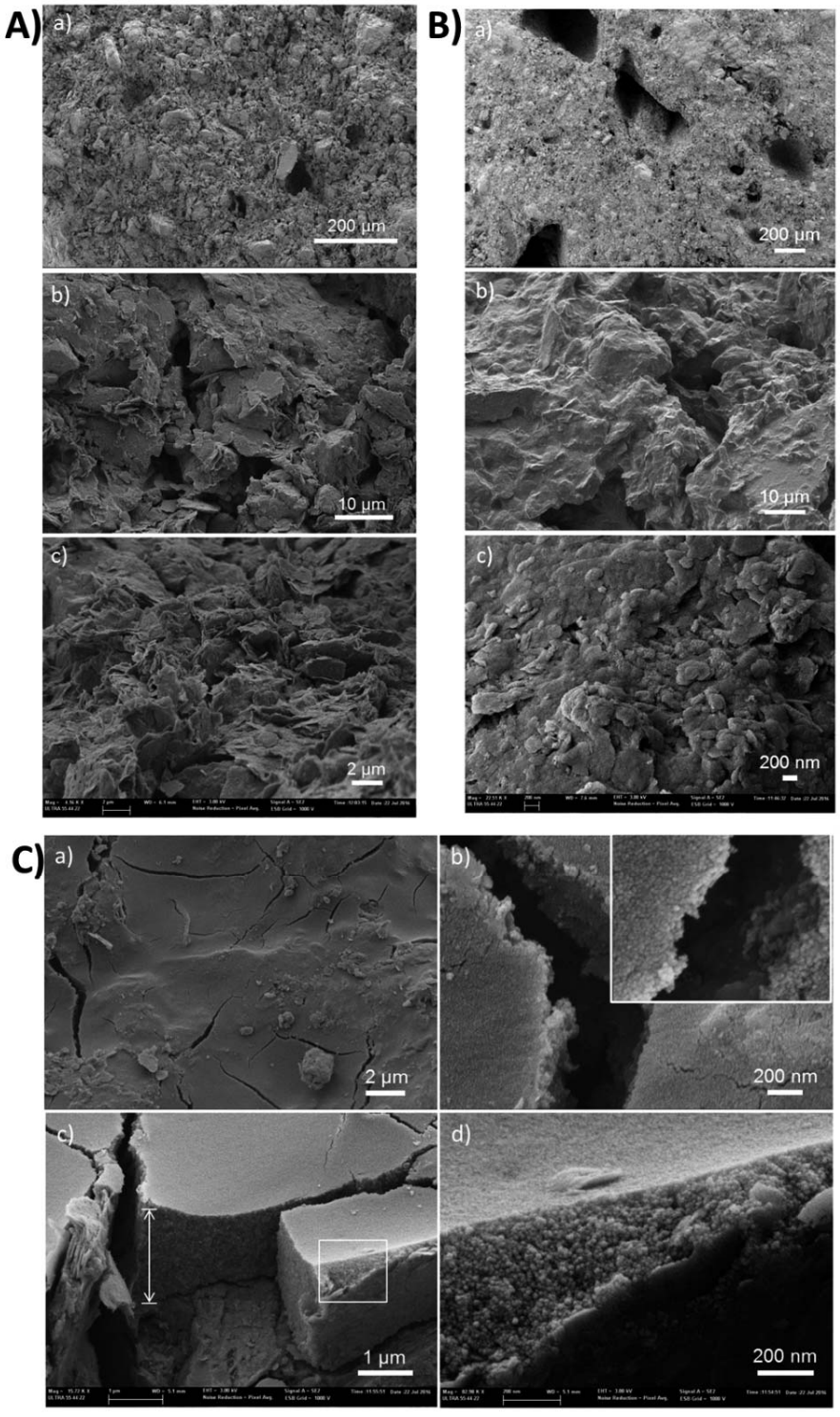

Fig. 7 FESEM secondary electron images of the microstructure of the **A)** untreated clay at three magnifications, B) treated with diluted nanoSiO_2 at different magnifications and **C)** residual layer on the surface of the treated pieces with non-diluted nanoSiO_2 suspension.

The analysis of the cross-section of the treated samples was also conducted. Fig. 7-B shows the microstructure of the cross-section of the treated clay with diluted nanoSiO_2. The cross-section was obtained at about 100μm from the surface. It revealed that the great pores previously detected by optical microscopy were not filled by the solid content of the consolidating substance, (Fig. 7-B a). Nevertheless, higher magnifications (Fig. 7-B b and c) reveal different microstructure than that of the untreated clay (Fig. 7-A). A smooth microstructure was observed and the single grains are not distinguished, suggesting that the solid content of the consolidating suspension has appropriately penetrated into the inter grains regions.

In the case of clays treated with undiluted suspension, the consolidating behavior was only observed onto the outside of the surface, showing that the solid content could not penetrate the clay material. The Fig. 7-C a, shows a cracked surface, in good accordance with the residual material observed in Fig. 7d attributed to the bad absorption generated by the high viscosity of the undiluted suspension. At higher magnifications (Fig. 7-C b, c and d) it is revealed the nanostructure of the deposited layer where nanoparticles can be distinguished.

These results, indicates that the use of the undiluted suspension leads to only a very surface consolidation since the high viscosity does not allows a homogeneous dispersion of nanoparticles into the clay matrix. Whereas, using a diluted suspension the nanoparticles were homogeneously diffused to the bulk of the clay achieving a more width consolidation treatment due to the ability of nanoparticles to enhance the interfacial adhesion.

In order to clarify how the nanoparticles are improving the interactions between the clay material and the consolidating suspension, several FESEM images were captured at very high magnification. Fig. 8 shows the FESEM images at two

magnifications acquired from the cross-section of treated clay with diluted nanoSiO_2. It can be seen that the nanoparticles were located not only between the laminar planes (Fig.8-a), but also between the basal planes (Fig. 8-b).

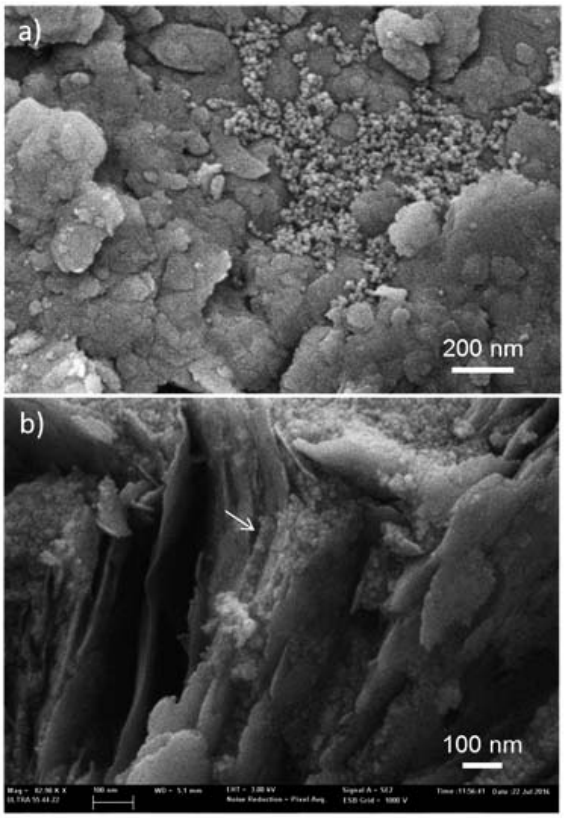

Fig. 8. FESEM images of the nano-SiO_2 particles in the clay microstructure.

This finding confirms that the nanoparticles were able to penetrate the clay's surface and also to fill the intergranular spaces, due to the fact that they are nanometric as well as due to the well dispersed nanoparticles in the diluted colloidal suspension. This fact favors the formation of a homogeneous material at the same time as it is expected that the nanoparticles interact with the clay matrix by means of different kind of interactions. The involved mechanism should be able to produce the formation of stronger physico-chemical interactions than the typical found in consolidated ancient clays, reducing the exfoliation character and, therefore, a greater resistance is expected.

3.3.2. Colorimetric analysis

The materials' colours are provided in a uniform colour scale, being the most used the CIELab scale because it is the most uniform colour space from a perceptual point of view [30]. In this work, the influence of the consolidated treatments on the surface colour was evaluated by scanning the samples under a unique capture, making sure that all samples receive the same lamp intensity, while light exposure and capture parameters remained the same. The captured images (not shown) were subsequently analyzed using professional photographic software. Table 3 summarizes the parameters obtained from the CIELab colour spaces the average value resulting from 25 tests performed at random positions over the images.

Table 3. Summary of the CIELa*b* characteristics of the analyzed samples

	Untreated	Nano Estel	Nano Estel/water v/v
L	74.4 ± 0.5[a]	65.8 ± 0.8[b]	65.9 ± 0.7[b]
a*	16.9 ± 0.8[a]	19.3 ± 0.8[a,b]	20.1 ± 0.8[b]
b*	23.2 ± 0.8[a]	25.5 ± 0.4[a]	20.1 ± 0.8[b]
ΔL	-	8.6 ± 0.3	-8.5 ± 0.2
Δa	-	2.4 ± 0.1	3.2 ± 0.1
Δb	-	2.3 ± 0.4	3.1 ± 0.1
ΔE	-	9.2 ± 0.5[a]	9.6 ± 0.2[a]

[a–b] Different superscripts within the same row indicate significant differences between formulations ($p < 0.05$).

These values indicate that the clay pieces have a low luminosity and are located in the quadrant of the CIELab space ranging from red to yellow. Moreover, positive values obtained for the a* coordinate indicate a deviation towards red, while positive values for the b* coordinate are indicative of a deviation towards yellow. The treatments have produced a small darkening effect (decrease in *L* values). A reddening and somewhat amber tonality was observed when increasing the concentration of the applied suspension, demonstrated by the increased values of a* and b* coordinates, respectively. No significant differences in total colour differences were observed between Nano Estel treated samples ($p > 0.05$), but they showed a slight difference with respect to untreated samples ($p < 0.05$). It should be noted that the total colour differences were higher than 2.0, being this value frequently used as a limit of the threshold of perceptible colour difference for the human eye [31]. Comparing the treated samples with the untreated one, it was possible to conclude that the trend towards red and yellow is significant in the case of the non-diluted suspension treatment. Nevertheless, this tendency is not significant when the colloidal nanoSiO_2 suspension was diluted in water. Note that working with clay objects this problem can be particularly difficult to deal with since color variations can be very evident

3.3.2. Hardness and Elastic Modulus characterization

The aim of this study was to evaluate the improvement on the mechanical resistance of the surfaces of ancient clay pieces by the addition of commercial SiO_2 nanoparticles. The nanoindentation technique has shown an important development to measure the mechanical properties of several kind of materials including metals [15, 32], ceramics [33-35] polymers [36-38] and wood products [39, 40]. This technique has been also successfully used to study the conservation state of fragile heritage objects

343 [20, 25, 31] and offer the possibility to study a small volume of material in order to
344 understand the conservation state of the entire piece [41]. The hardness (H) and elastic
345 modulus (E) of these pieces were measured under very low loads using a nanoindenter.
346 Fig. 9-a and b, shows the H and E in-depth profiles acquired for each analyzed sample.

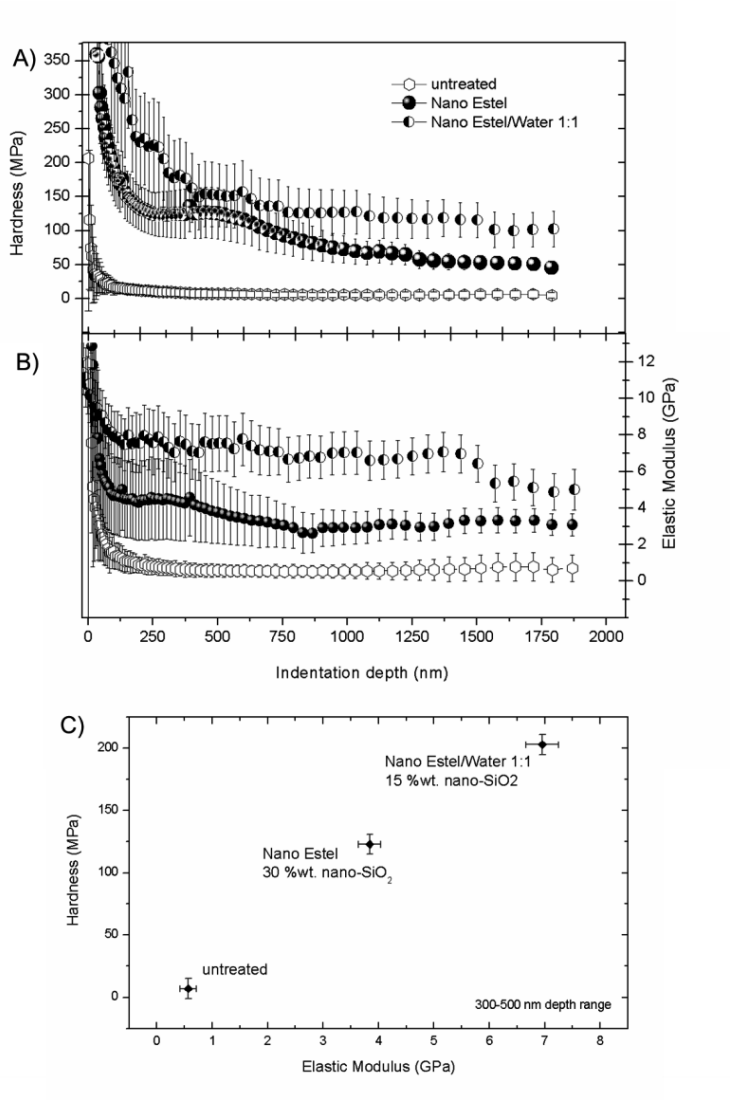

347

348 **Fig. 9.** Nanoindentation results of untreated and treated samples in-depth: **a)** Hardness
349 profile, **b)** elastic modulus profile and **c)** H vs. E values averaged over the 300-500 nm
350 depth.

351

352 It's important to clarify that these nanoindentation curves are consequence to
353 superficially indent a very small volume of material, assuring us that the piece is not

damaged by the test and that only the treated surface is measured. This is, the penetration capacity achieved by the treatment isn't able to be detected under the experimental conditions used in this study because this feature is out of the aim of this work (this penetration capacity should be difficult to be extrapolated to the behavior of the same material in other conditions of porosity, chemical composition, etc). These curves reveal that the untreated samples have a mean hardness of 15 MPa and an elastic modulus of 1 GPa. Nevertheless, samples treated with the concentrated suspension shifted these curves to higher values, reaching 140 MPa and 5 GPa for H and E, respectively. Nonetheless, the hardening effect for this case (concentrated suspension) was only found over a shallow depth of ~600 nm. Once this depth is reached, the H and E values tend to decrease, indicating that the treatment did not deepen beyond this point, it agreeing with the conclusions obtained from the microstructure analysis performed by FESEM previously commented. In this sense, when the nano-SiO_2 colloidal suspension was diluted in distilled water, the hardness and elastic modulus reached higher values, 150 MPa and 8 GPa, respectively. As conclusion, the absorption of SiO_2 particles increased the hardness and the moduli of the material, while it is required to dilute the concentration of solid content in the suspension in order to improve its penetration and to obtain an appropriate distribution. Considering the effect of the treatment as a result of a surface effect (first nanometers in depth), these results were averaged in the range of 300-500 nm in depth, as shown in Fig.9-c.

3.3.3. Friction surface's resistance characterization

The advantage of the scratch test is that it allows determining the friction resistance of the materials and can be considered as particular hardness measurement. The concept of the scratch hardness complements the resistance behavior of any ancient

379 material as only small friction forces must be permitted during the conservation-
380 restoration procedure. A scratch procedure consists on moving the sample underneath
381 the indenter while a normal force is ramped. The result of this process is the generation
382 of a tangential force which scratches the specimen while special sensors register the
383 depth and friction force of the induced track.
384 The steps programmed for this experiment where the following: (i) a pre-scan of the
385 path topography using very low loads, (ii) a ramp of load that is linearly applied during
386 the programmed path, and (iii) a post-profile scan that is performed in order to acquire
387 the residual depth of the newly created track. Fig. 10-a, shows the residual cross-
388 profiles acquired on each scratched surface at 250 μm of the generated path (at ~1.75
389 mN scratch load). It is corroborated that the depth and hence, the damage provoked on
390 the untreated sample is significantly higher than in treated samples. The generated
391 groove on untreated samples reached 15 μm depth, versus the 5 and 8 μm for the treated
392 surface with diluted and non-diluted suspension, respectively.

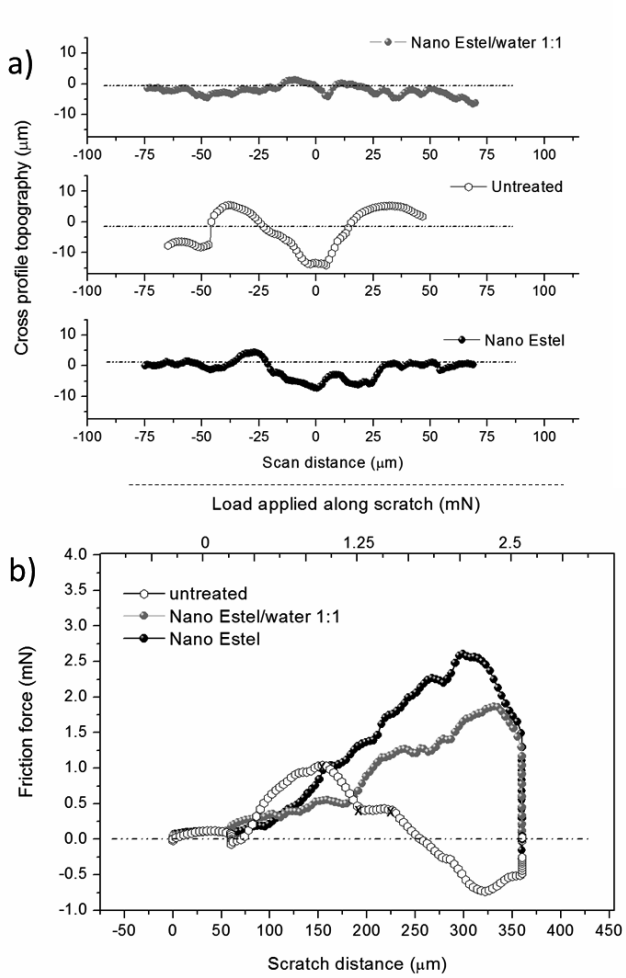

393

394 **Fig. 10.** a) Cross-profile scans acquired after the scratch test at 150 μm of path, b)
395 friction force curves acquired during the scratch tests.

396

397 In the absence of a significant failure mechanism, the friction force is linearly
398 dependent on the normal force applied. The value of the resultant force depends of the
399 coefficient of friction between materials. The friction forces registered along the scratch
400 test for each sample are showed in Fig. 10-b. As can be seen on this figure, the friction
401 force acquired on the untreated sample drop set a 150 μm scratch distance, indicating
402 that the material failed at the critical ~1 mN scratch load. However, the surfaces treated
403 with nano-SiO_2 revealed a continuous increase of friction without an observable failure
404 mechanism, corroborating the consolidation effect. The higher friction force recorded in

405 the sample treated with non-diluted suspension is explained by the excess of non-
406 absorbed nano-silica that produces an adhesive effect.
407
408 The evidences of this study show that a treatment with an aqueous colloidal
409 suspension of nano-SiO_2 particles improves the mechanical resistance of the surfaces of
410 non-consolidated clay pieces. This behavior could be attributed to the ability of nano-
411 SiO_2 particles to harden the clay since they flow to the micro-cavities of the low dense
412 clay microstructure, it leading to physical-chemical interactions between the
413 nanoparticles and the consolidated material. The nanoparticles filled the narrow inter-
414 grain spaces, while the use of them diluted and dispersed in a water solution contributes
415 to improve their homogeneous distribution and their well dispersion allows the
416 enhancement of the interfacial adhesion in the final consolidated nanocomposite. In this
417 stage, the well dispersed nanoparticles are able to interact with the terminal charges
418 molecules of the clay matrix, such as hydroxides, aluminates, or other silicates, present
419 in the clay. Regardless it is widely known that the use of nanoparticles instead of larger
420 sized particles (i.e.: microparticles) is preferred not only due to their higher surface area
421 that allows better interaction with the material, but also due to the fact of if they are well
422 dispersed they are easily transported within the porous of the treated material. In further
423 studies it should search for the optimum dilution ratio in order to treat historical samples
424 with the lowest amount of silica needed to obtain the required final performances.
425
426
427 **4- Conclusions**
428 Brittle and ancient clay surfaces were successfully strengthened with a special
429 surface treatment consisting of a colloidal suspension of nano-SiO_2. TEM images

corroborated that the diameters of particle were below 20nm. Meanwhile, FESEM images confirmed that the diffusion of the nanoparticles to the bulk of the clay depends on the concentration of the consolidating substance. Moreover, it was found that the SiO_2 nanoparticles are able to fill the inter-granular spaces of the laminar microstructure of the ancient clay pieces, enhancing the interfacial adhesion and, thus, improving the final mechanical performance. The nanoindentation technique has been confirmed as a powerful, non-destructive method that can measure the hardness, elastic modulus and scratch resistance of delicate surfaces of ancient pieces. The dispersed SiO_2 nanoparticles were able to enhance the interfacial adhesion grains/nanofiller and, thus increasi the friction resistance and hardness (from 15 MPa to 150 MPa) and the elastic modulus (from 1 to 8 GPa) for untreated and treated surfaces, respectively. However, the required concentration to improve the mechanical resistance affects the visual appearance of the clays by slightly darkening the surface of the ancient clays.

ACKNOWLEDGEMENTS

Authors acknowledge the financial support of Spanish Ministry of Economy and Competitiveness, MAT2014-59242-C2-1-R. Authors also acknowledge the support of Helena Bonet, Director of the Prehistory Museum of Valencia and Mª Jesús de Pedro, conservator of this Museum, and to the Photographic Archive Department. M.P. Arrieta wishes to thank the financial support of MINECO for a Juan de la Cierva (FJCI-2014-20630) contract.

References

[1] A. Adriaens, M.G. Dowsett, Applications of SIMS to cultural heritage studies, Applied Surface Science 252(19) (2006) 7096-7101.

[2] V. Crupi, G. Galli, M.F. La Russa, F. Longo, G. Maisano, D. Majolino, M. Malagodi, A. Pezzino, M. Ricca, B. Rossi, S.A. Ruffolo, V. Venuti, Multi-technique investigation of Roman decorated plasters from Villa dei Quintili (Rome, Italy), Applied Surface Science 349 (2015) 924-930.

[3] E. Fazio, S. Trusso, R.C. Ponterio, Surface-enhanced Raman scattering study of organic pigments using silver and gold nanoparticles prepared by pulsed laser ablation, Applied Surface Science 272 (2013) 36-41.

[4] A. Gianoncelli, J. Castaing, L. Ortega, E. Dooryhée, J. Salomon, P. Walter, J.L. Hodeau, P. Bordet, A portable instrument for in situ determination of the chemical and phase compositions of cultural heritage objects, X-Ray Spectrometry 37(4) (2008) 418-423.

[5] J.L. Perez-Rodriguez, A. Duran, Mineralogical characterization of the polychrome in cultural heritage artifacts (antiquity to date) from southern spain using micro-raman spectroscopy and complementary techniques, Spectroscopy Letters 47(3) (2014) 223-237.

[6] J.L. Perez-Rodriguez, M.D. Robador, M.C.J.D. Haro, J.M.M. Blanes, I. Garofano, C. Odriozola, A. Duran, Non-invasive analytical techniques applied to characterize the components of ancient golden medallions, Heritage Science 1(1) (2013).

[7] A.V. Rode, K.G.H. Baldwin, A. Wain, N.R. Madsen, D. Freeman, P. Delaporte, B. Luther-Davies, Ultrafast laser ablation for restoration of heritage objects, Applied Surface Science 254(10) (2008) 3137-3146.

[8] A. Duran, L.A. Perez-Maqueda, J. Poyato, J.L. Perez-Rodriguez, A thermal study approach to roman age wall painting mortars, Journal of Thermal Analysis and Calorimetry 99(3) (2010) 803-809.

[9] G. Politi, A. Bouquillon, M. Aucouturier, A. Gueli, S.O. Troja, C. Vella, C. Pacheco, L. Pichon, B. Moignard, Q. Lemasson, Analysis of lustred ceramics of the Galleria Regionale di Palazzo Bellomo di Siracusa, Italy, Nuclear Instruments and Methods in Physics Research Section B: Beam Interactions with Materials and Atoms 331 (2014) 82-88.

[10] A. Polvorinos, M. Aucouturier, A. Bouquillon, J. Castaing, J. Camps, THE EVOLUTION OF LUSTRE CERAMICS FROM MANISES (VALENCIA, SPAIN) BETWEEN THE 14TH AND 18TH CENTURIES, Archaeometry 53(3) (2011) 490-509.

[11] C.D. Vito, L. Medeghini, S. Mignardi, P. Ballirano, L. Peyronel, Technological fingerprints of the Early Bronze Age clay figurines from Tell Mardikh-Ebla (Syria), Journal of the European Ceramic Society 35(13) (2015) 3743-3754.

[12] N. Wang, L. He, E. Egel, S. Simon, B. Rong, Complementary analytical methods in identifying gilding and painting techniques of ancient clay-based polychromic sculptures, Microchemical Journal 114 (2014) 125-140.

[13] A. Duran, I. Navarro-Blasco, J.M. Fernández, J.I. Alvarez, Long-term mechanical resistance and durability of air lime mortars with large additions of nanosilica, Construction and Building Materials 58 (2014) 147-158.

[14] K.A. Padmanabhan, Mechanical properties of nanostructured materials, Materials Science and Engineering: A 304–306 (2001) 200-205.

[15] V. Bonache, E. Rayón, M.D. Salvador, D. Busquets, Nanoindentation study of WC–12Co hardmetals obtained from nanocrystalline powders: Evaluation of hardness and modulus on individual phases, Materials Science and Engineering: A 527(12) (2010) 2935-2941.

[16] C. Rao, Chemistry of Nanomaterials, World Scientific, Bangalore, India, 2014.

[17] M.F. La Russa, S.A. Ruffolo, N. Rovella, C.M. Belfiore, P. Pogliani, C. Pelosi, M. Andaloro, G.M. Crisci, Cappadocian ignimbrite cave churches: Stone degradation and conservation strategies, Periodico di Mineralogia 83(2) (2014) 187-206.

[18] R. Giorgi, M. Baglioni, D. Berti, P. Baglioni, New Methodologies for the Conservation of Cultural Heritage: Micellar Solutions, Microemulsions, and Hydroxide Nanoparticles, Accounts of Chemical Research 43(6) (2010) 695-704.

[19] R. Giorgi, M. Ambrosi, N. Toccafondi, P. Baglioni, Nanoparticles for Cultural Heritage Conservation: Calcium and Barium Hydroxide Nanoparticles for Wall Painting Consolidation, Chemistry – A European Journal 16(31) (2010) 9374-9382.

[20] R.-M. Ion, S.M. Doncea, M.-L. Ion, V. Rădiţoiu, V. Amăriuţei, Surface investigations of old book paper treated with hydroxyapatite nanoparticles, Applied Surface Science 285, Part A (2013) 27-32.

[21] J.C.D.A. de Figueiredo Junior, S.S. Asevedo, J.H.R. Barbosa, Removal of brownish-black tarnish on silver–copper alloy objects with sodium glycinate, Applied Surface Science 317 (2014) 67-72.

[22] J.M. Fernández, A. Duran, I. Navarro-Blasco, J. Lanas, R. Sirera, J.I. Alvarez, Influence of nanosilica and a polycarboxylate ether superplasticizer on the performance of lime mortars, Cement and Concrete Research 43 (2013) 12-24.

524 [23] A. Ferron, F.G. Matero, A comparative study of ethyl-silicate-based consolidants
525 on earthen finishes, Journal of the American Institute for Conservation 50(1)
526 (2011) 49-72.
527 [24] J. Salvant, E. Barthel, M. Menu, Nanoindentation and the micromechanics of Van
528 Gogh oil paints, Applied Physics A: Materials Science and Processing 104(2)
529 (2011) 509-515.
530 [25] E. Barna, B. Bommer, J. Kürsteiner, A. Vital, O.v. Trzebiatowski, W. Koch, B.
531 Schmid, T. Graule, Innovative, scratch proof nanocomposites for clear coatings,
532 Composites Part A: Applied Science and Manufacturing 36(4) (2005) 473-480.
533 [26] C. Salgado, M.P. Arrieta, L. Peponi, M. Fernández-García, D. López, Silica-
534 nanocomposites of photo-crosslinkable poly(urethane)s based on poly(ε-
535 caprolactone) and coumarin, European Polymer Journal 93 (2017) 21-32.
536 [27] M. De Pedro, la lloma de betxí. un poblado de la edad del bronce (paterna,
537 Valencia), Trabajos Varios del SIP, 1998.
538 [28] J.A. López Mira, De hilos, telares y tejidos en el Argar alicantino, En los confines
539 del Argar: una cultura de la Edad del Bronce en Alicante en el centenario de Julio
540 Furgús:[exposición], Museo Arqueológico de Alicante-MARQ, 2009, pp. 136-
541 153.
542 [29] E. Rayón, V. Bonache, M. Salvador, E. Bannier, E. Sánchez, A. Denoirjean, H.
543 Ageorges, Nanoindentation study of the mechanical and damage behaviour of
544 suspension plasma sprayed TiO 2 coatings, Surface and Coatings Technology
545 206(10) (2012) 2655-2660.
546 [30] Ó. Lantes-Suárez, B. Prieto, M.P. Prieto-Martínez, C. Ferro-Vázquez, A. Martínez-
547 Cortizas, The colour of ceramics from Bell Beaker contexts in NW Spain: relation
548 to elemental composition and mineralogy, Journal of Archaeological Science 54
549 (2015) 99-109.
550 [31] M.P. Arrieta, E. Fortunati, F. Dominici, E. Rayón, J. López, J.M. Kenny, PLA-
551 PHB/cellulose based films: mechanical, barrier and disintegration properties,
552 Polymer Degradation and Stability 107 (2014) 139-149.
553 [32] J.J. Roa, M. Martínez, E. Rayón, N. Ferrer, F. Espiell, M. Segarra, Hardness of
554 FRHC-Cu determined by statistical analysis, Journal of Materials Engineering and
555 Performance 23(2) (2014) 637-642.
556 [33] P. Carpio, E. Rayón, M.D. Salvador, L. Lusvarghi, E. Sánchez, Mechanical
557 Properties of Double-Layer and Graded Composite Coatings of YSZ Obtained by

Atmospheric Plasma Spraying, Journal of Thermal Spray Technology 25(4) (2016) 778-787.

[34] G. Oncins, J.J. Roa, E. Rayón, J. Díaz, M. Morales, M. Segarra, F. Sanz, Friction, hardness and elastic modulus determined by AFM-FS and nanoindentation techniques for advanced ceramics materials, Recent Advances in Ceramic Materials Research2013, pp. 215-249.

[35] J.J. Roa, A. Magrasó, M. Morales, P. Núñez, M. Segarra, Determination of hardness, Young's modulus and fracture toughness of lanthanum tungstates as novel proton conductors, Ceramics International 37(5) (2011) 1593-1599.

[36] M.P. Arrieta, M.D.M. Castro-López, E. Rayón, L.F. Barral-Losada, J.M. López-Vilariño, J. López, M.V. González-Rodríguez, Plasticized poly(lactic acid)-poly(hydroxybutyrate) (PLA-PHB) blends incorporated with catechin intended for active food-packaging applications, Journal of Agricultural and Food Chemistry 62(41) (2014) 10170-10180.

[37] M.P. Arrieta, J. López, A. Hernández, E. Rayón, Ternary PLA-PHB-Limonene blends intended for biodegradable food packaging applications, European Polymer Journal 50(1) (2014) 255-270.

[38] A. Flores, F. Ania, H.J. Salavagione, G. Ellis, D. Saurel, M.A. Gómez-Fatou, Local mechanical properties of graphene/polyethylene-based nanocomposites by depth-sensing indentation, European Polymer Journal 74 (2016) 120-129.

[39] E. Rayón, S. Ferrandiz, M.I. Rico, J. López, M.P. Arrieta, Microstructure, mechanical, and thermogravimetric characterization of cellulosic by-products obtained from biomass seeds, International Journal of Food Properties 18(6) (2015) 1211-1222.

[40] E. Rayón, J. López, M.P. Arrieta, Mechanical characterization of microlaminar structures extracted from cellulosic materials using nanoindentation technique, Cellulose Chemistry and Technology 47(5-6) (2013) 345-351.

[41] T.K. Bader, K. de Borst, K. Fackler, T. Ters, S. Braovac, A nano to macroscale study on structure-mechanics relationships of archaeological oak, Journal of Cultural Heritage 14(5) (2013) 377-388.

Clay pieces of the Bronce Age

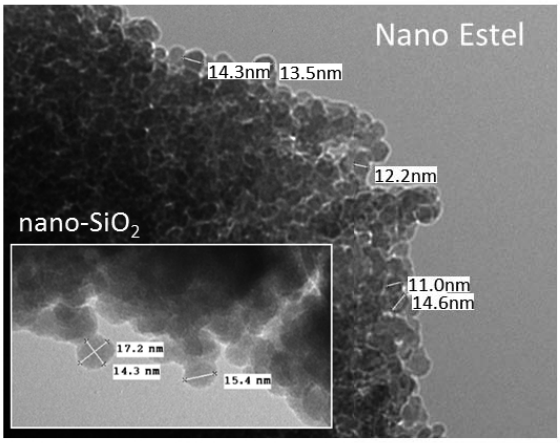

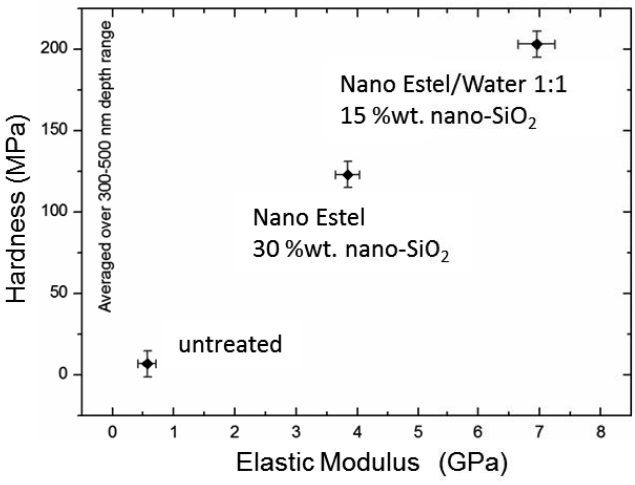


1cm / div

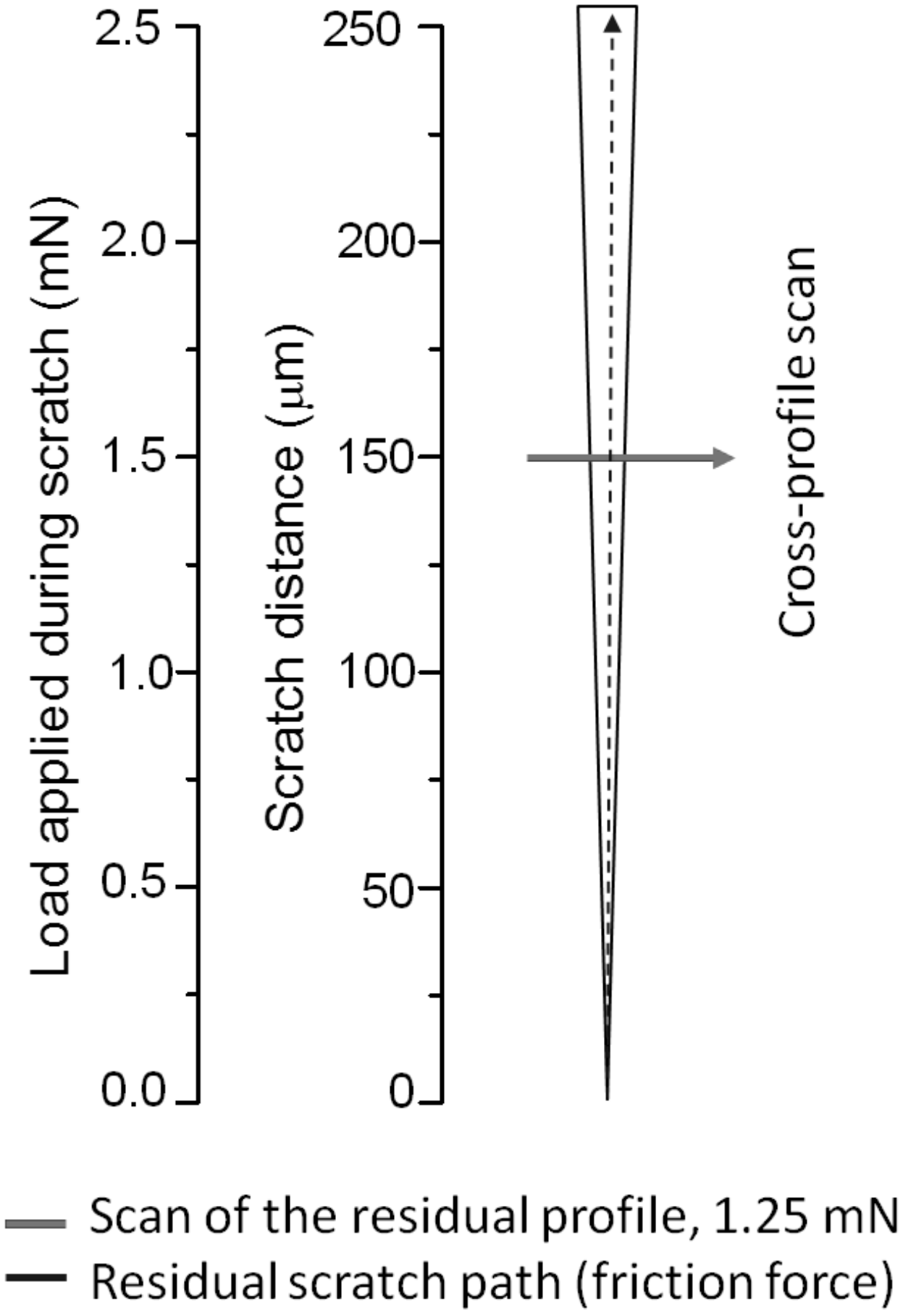
2.5
2.0
1.5
1.0
0.5
0.0
Load applied during scratch (mN)
250
200
150
100
50
0
Scratch distance (μm)
Cross-profile scan
Scan of the residual profile, 1.25 mN
Residual scratch path (friction force)

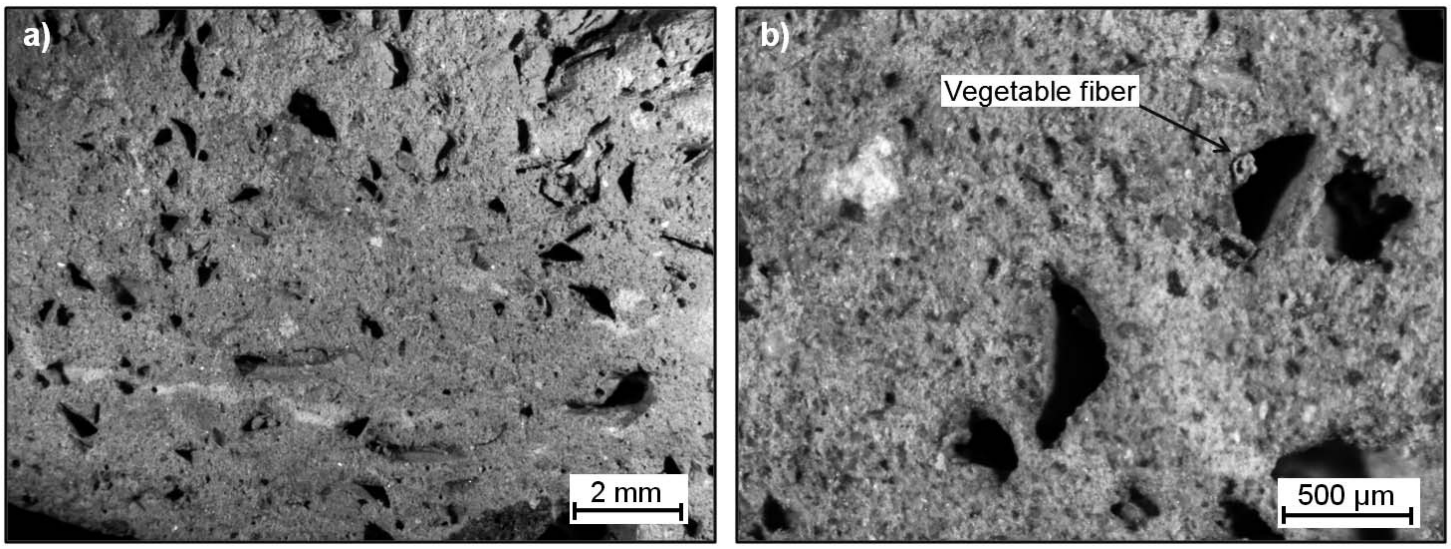
a)
2 mm
b)
Vegetable fiber
500 µm

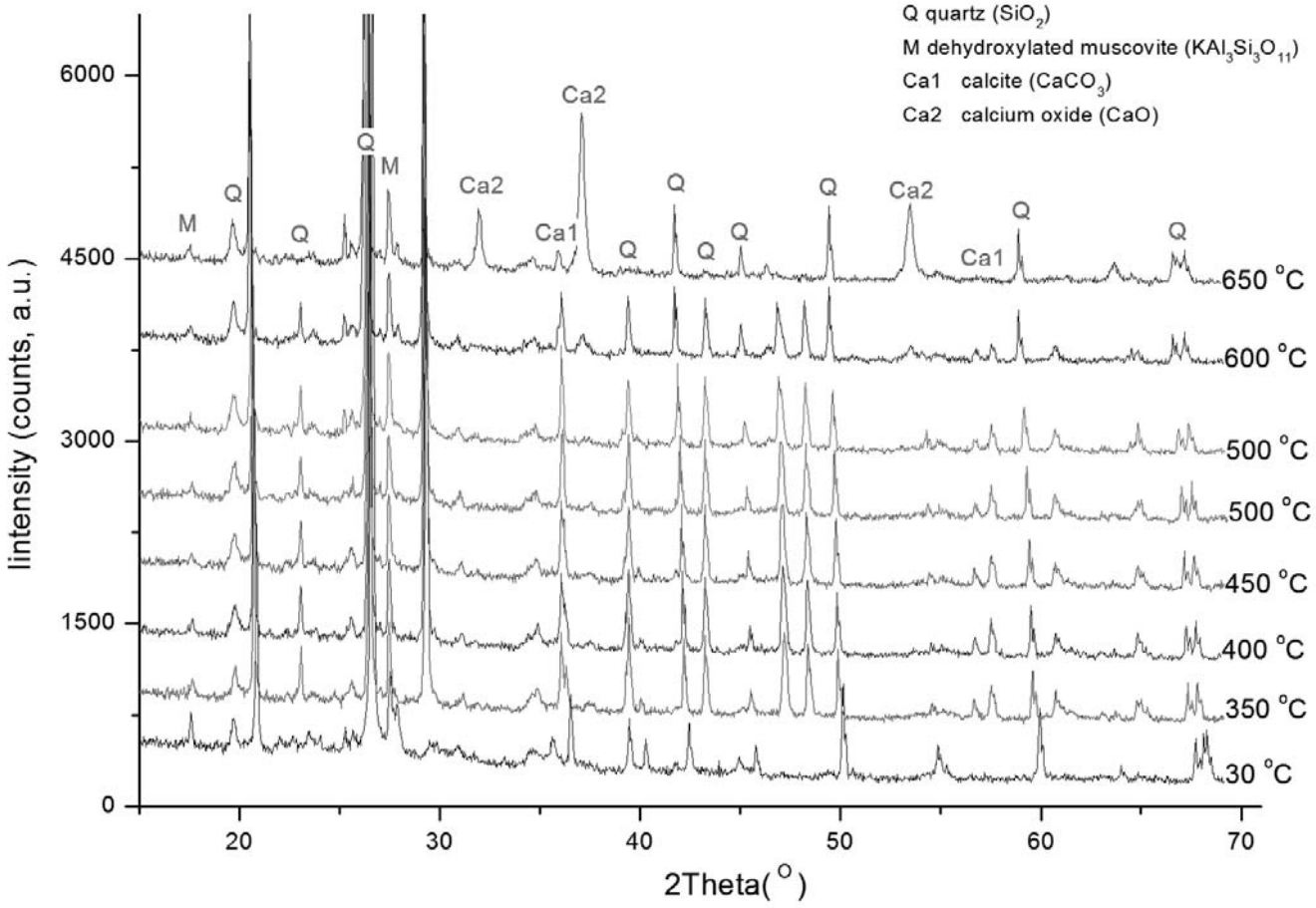
Q quartz (SiO_2)
M dehydroxylated muscovite ($KAl_3Si_3O_{11}$)
Ca1 calcite ($CaCO_3$)
Ca2 calcium oxide (CaO)
Intensity (counts, a.u.)
2Theta(°)
650 °C
600 °C
500 °C
500 °C
450 °C
400 °C
350 °C
30 °C

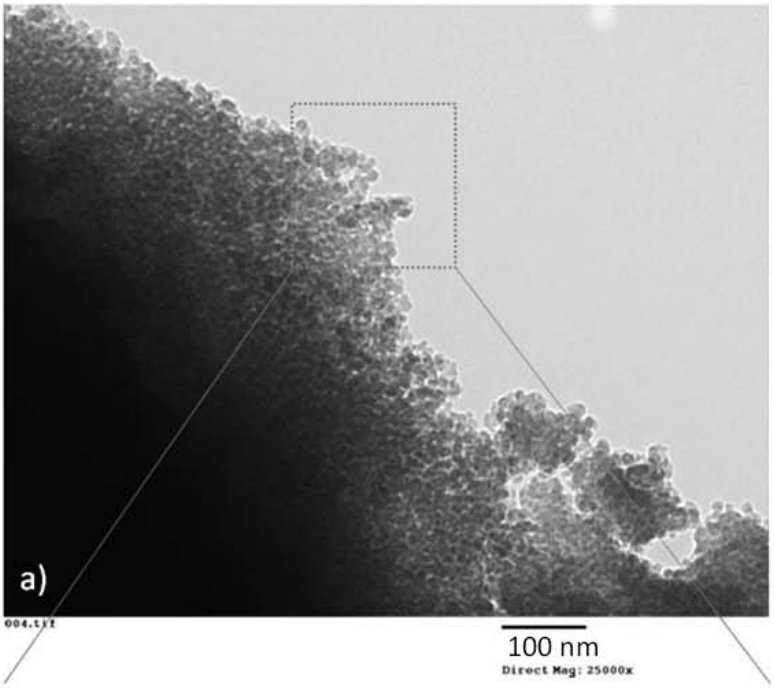
a)
004.tif
100 nm
Direct Mag: 25000x

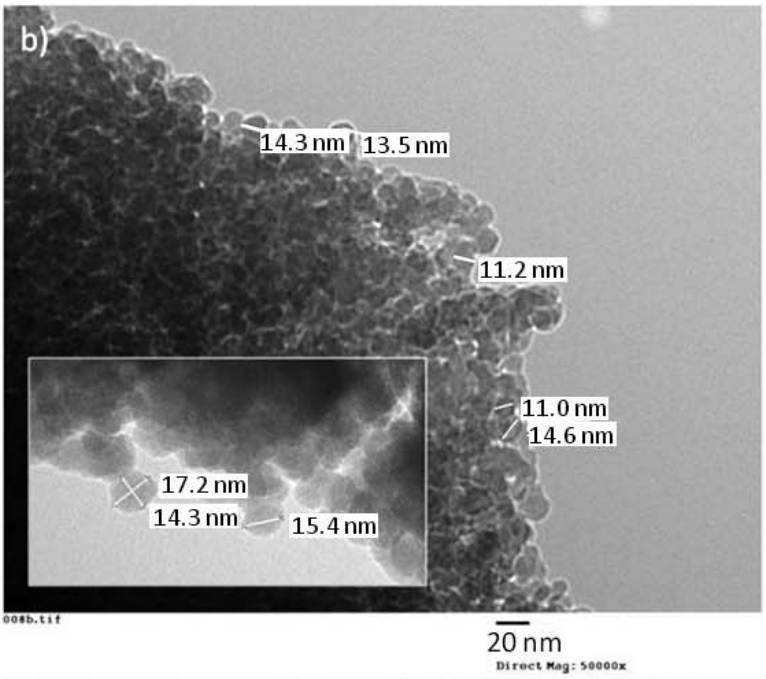
b)
14.3 nm
13.5 nm
11.2 nm
11.0 nm
14.6 nm
17.2 nm
14.3 nm
15.4 nm
008b.tif
20 nm
Direct Mag: 50000x

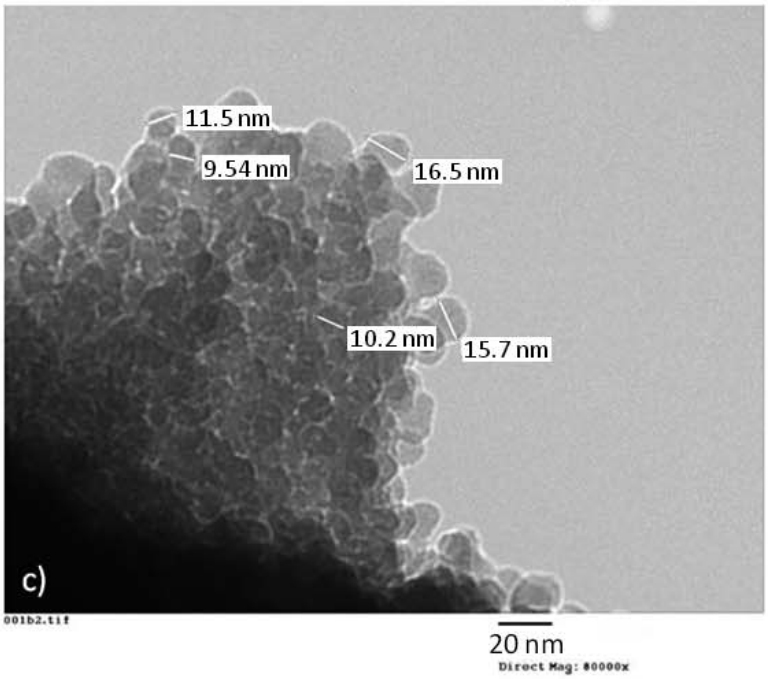
11.5 nm
9.54 nm
16.5 nm
10.2 nm
15.7 nm
c)
001b2.tif
20 nm
Direct Mag: 80000x

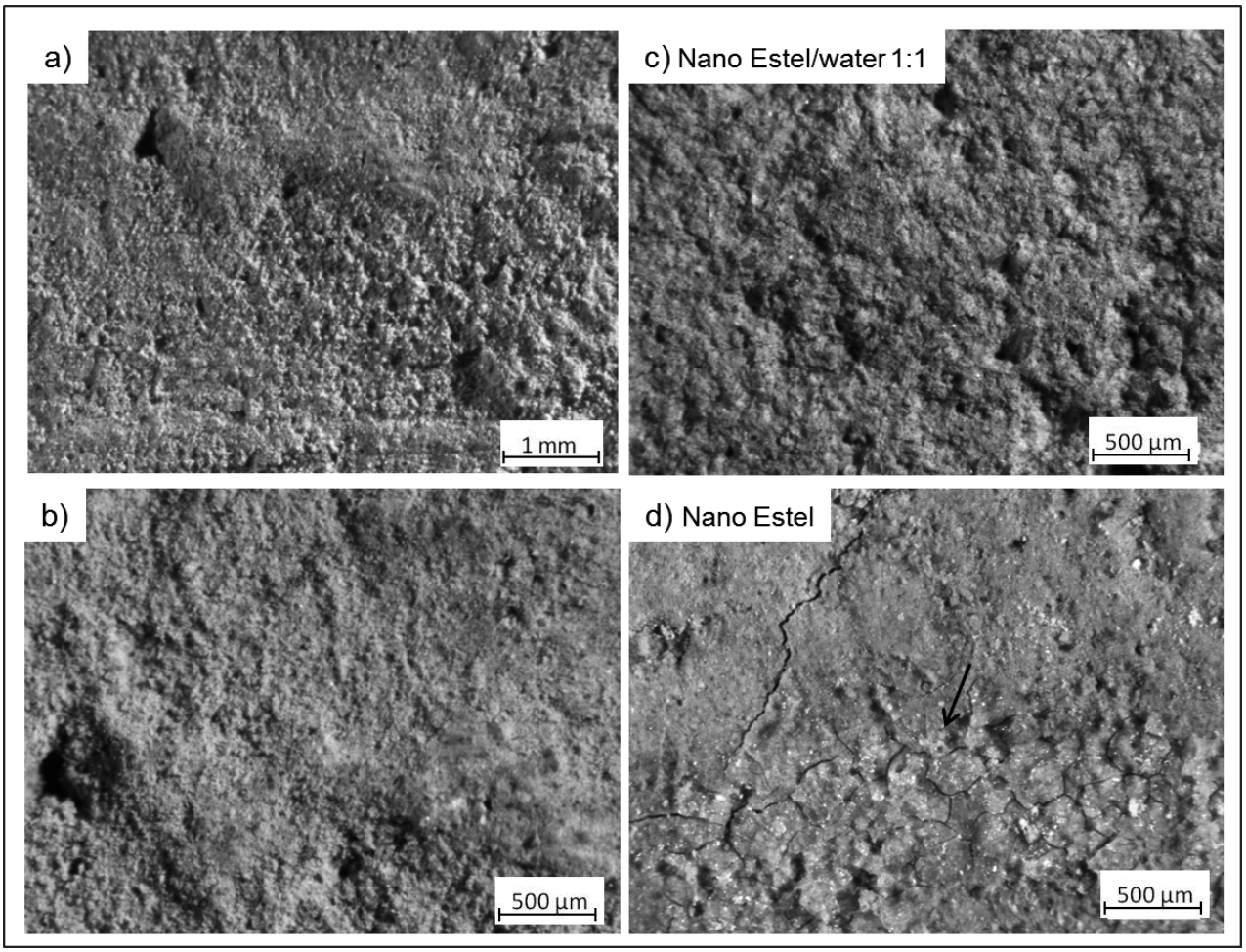
a)
1 mm
c) Nano Estel/water 1:1
500 µm
b)
500 µm
d) Nano Estel
500 µm

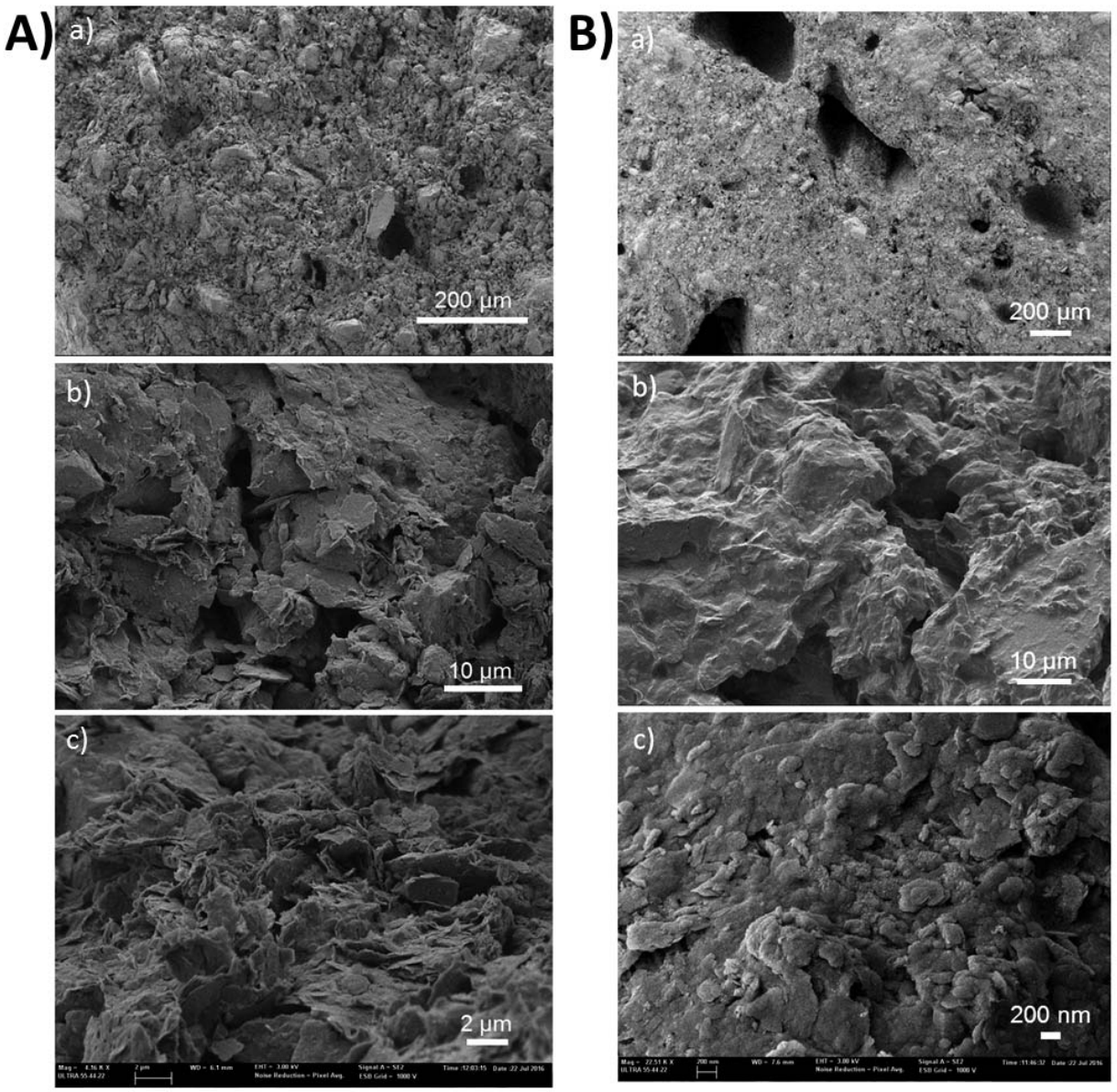
A)
a)
200 µm
b)
10 µm
c)
2 µm
B)
a)
200 µm
b)
10 µm
c)
200 nm

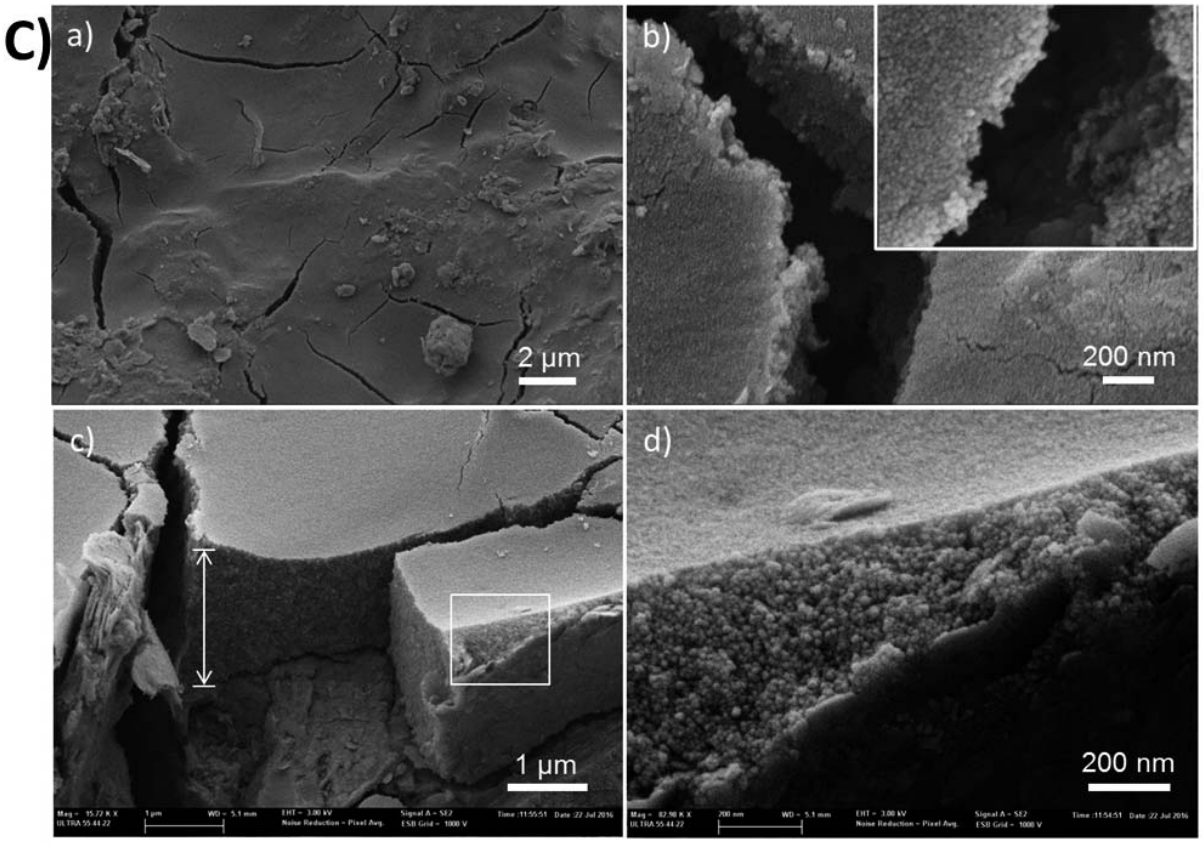
C)
a)
2 µm
b)
200 nm
c)
1 µm
d)
200 nm

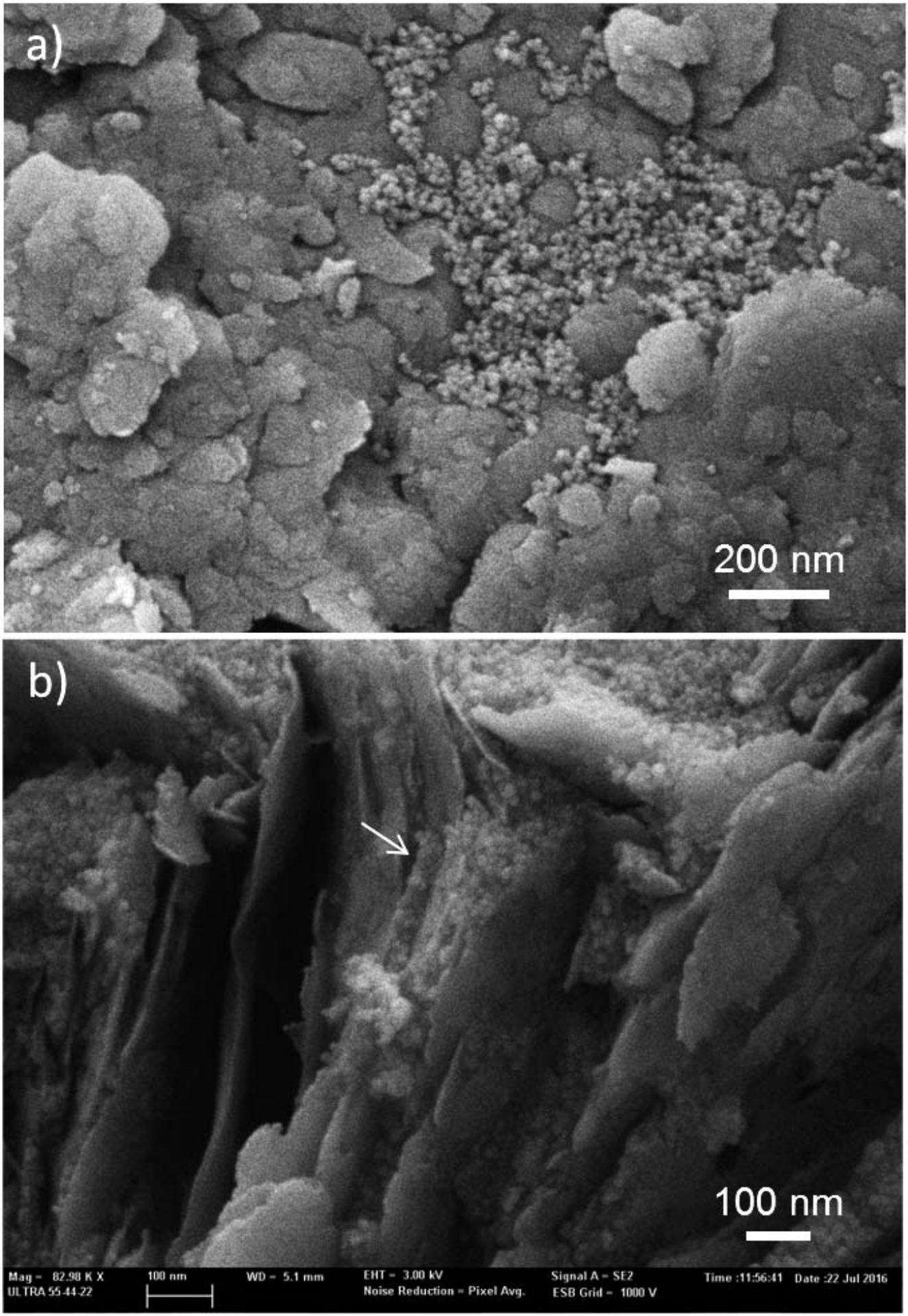
a)
200 nm
b)
100 nm
Mag = 82.98 K X
ULTRA 55-44-22
100 nm
WD = 5.1 mm
EHT = 3.00 kV
Noise Reduction = Pixel Avg.
Signal A = SE2
ESB Grid = 1000 V
Time :11:56:41 Date :22 Jul 2016

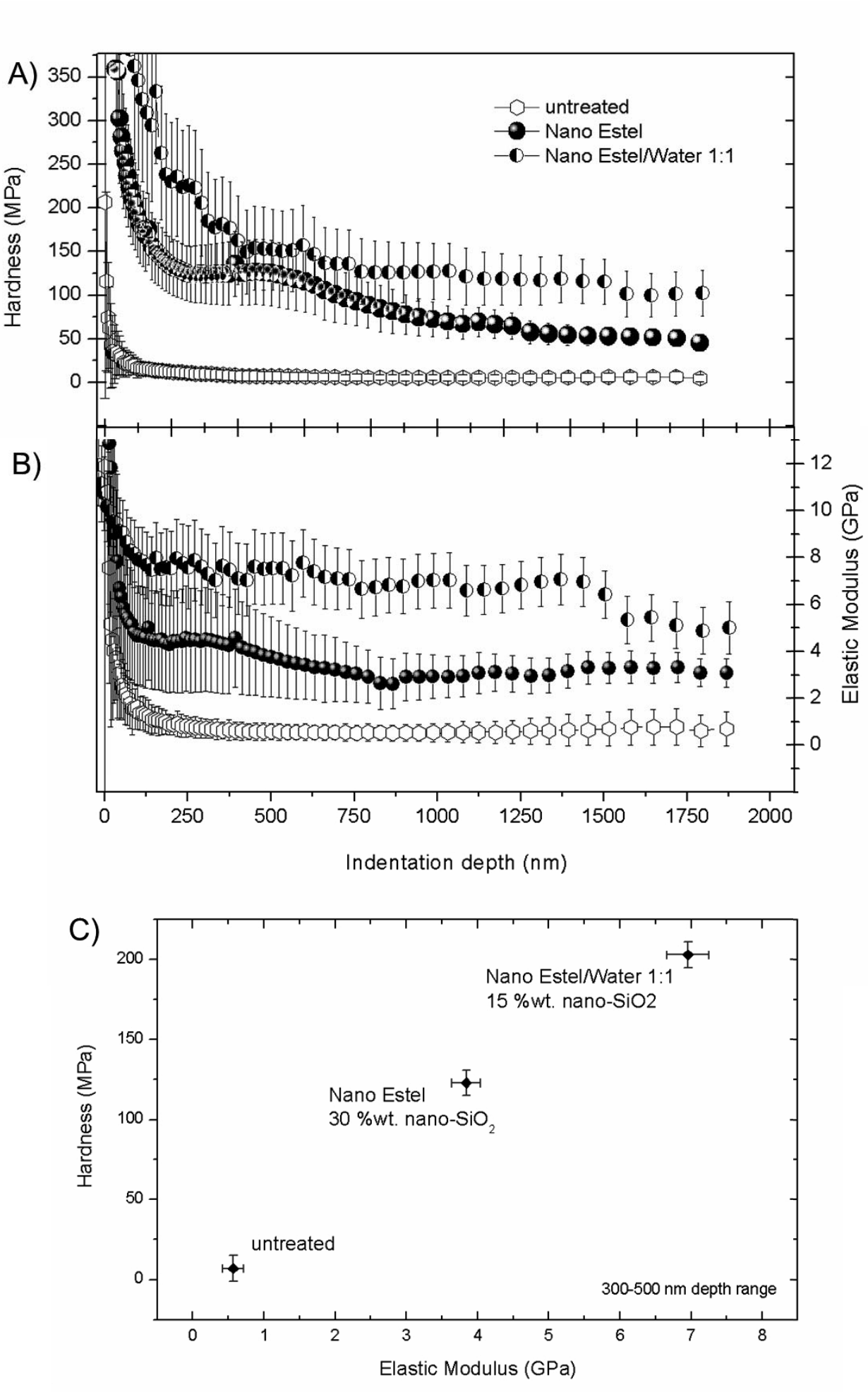
A)
B)
C)
untreated
Nano Estel
Nano Estel/Water 1:1
Hardness (MPa)
Elastic Modulus (GPa)
Indentation depth (nm)
Nano Estel/Water 1:1
15 %wt. nano-SiO2
Nano Estel
30 %wt. nano-SiO2
untreated
300-500 nm depth range

Nano Estel specifications	**Physical and chemical properties**
Solid material	SiO_2
Appearance	Colourless liquid
Solid content	30 wt%
Viscosity	7 mPa s at 20 ºC
Density	1.2 g / cm^3 at 20 ºC
Particle dimension	< 20 nm
Specific surface	260 m^2 / g
pH	10

Table 1. Summary of the physical and chemical properties of the commercial nano-SiO_2 suspension.

Element	Weight%	Atomic%
Mg	1.46	1.32
Al	10.58	8.58
Si	24.71	19.25
K	4.23	2.37
Ca	10.48	5.72
Fe	3.34	1.31
O	44.80	61.27

Table 2. Elemental analysis results of the clay material obtained by EDS-FESEM

Table 3. Summary of the CIELa*b* characteristics of the analyzed samples

	Untreated	Nano Estel	Nano Estel/water v/v
L	74.4 ± 0.5[a]	65.8 ± 0.8[b]	65.9 ± 0.7[b]
a*	16.9 ± 0.8[a]	19.3 ± 0.8[a,b]	20.1 ± 0.8[b]
b*	23.2 ± 0.8[a]	25.5 ± 0.4[a]	20.1 ± 0.8[b]
ΔL	-	8.6 ± 0.3	-8.5 ± 0.2
Δa	-	2.4 ± 0.1	3.2 ± 0.1
Δb	-	2.3 ± 0.4	3.1 ± 0.1
ΔE	-	9.2 ± 0.5[a]	9.6 ± 0.2[a]

[a–b] Different superscripts within the same row indicate significant differences between formulations ($p < 0.05$).